



# In-situ fabrication of reduced graphene oxide/leucomethylene blue/platinum nanoparticles modified electrode for voltammetric determination of trace Fe(II) in seawater



Su Ma<sup>a</sup>, Dawei Pan<sup>b,c,\*</sup>, Hong Wei<sup>a</sup>, Ning Wang<sup>b</sup>, Fei Pan<sup>b,c</sup>, Qi Kang<sup>a,\*\*</sup>

<sup>a</sup> College of Chemistry, Chemical Engineering and Materials Science, Key Laboratory of Molecular and Nano Probes, Ministry of Education, Shandong Provincial Key Laboratory of Clean Production of Fine Chemicals, Shandong Normal University, Jinan 250014, PR China

<sup>b</sup> Key Laboratory of Coastal Environmental Processes and Ecological Remediation, Yantai Institute of Coastal Zone Research, Chinese Academy of Sciences, Yantai 264003, PR China

<sup>c</sup> University of Chinese Academy of Sciences, Beijing 100049, PR China

## ARTICLE INFO

### Keywords:

In-situ fabrication  
Fe(II)  
Seawater  
Reduced graphene oxide  
Leucomethylene blue

## ABSTRACT

In this work, the modified electrode based on composites of reduced graphene oxide/leucomethylene blue/platinum nanoparticles (rGO/LMB/PtNPs) was fabricated in-situ via an electron relay effect. Cationic dye of methylene blue (MB) was absorbed on the surface of graphene oxide (GO) with through  $\pi$ - $\pi$  bond interactions. Then  $\text{PtCl}_6^{2-}$  ions were self-assembled on the surface of the composites of GO/MB through Coulomb interactions. Using  $\text{NaBH}_4$  as the reducing agent, PtNPs were formed and GO was reduced to rGO. With the aid of PtNPs, MB was catalytically degraded to LMB and a rGO/LMB/PtNPs modified electrode was successfully prepared in situ. Due to the excellent electrochemical properties of rGO and the well-established assistant reductant of MB, as well as the catalytic amplifying effect of PtNPs, this as prepared rGO/LMB/PtNPs modified electrode showed excellent properties for the voltammetric determination of Fe(II) with the linear range of 0.01 to 2  $\mu\text{M}$  and a detection limit of 3 nM. This modified electrode was successfully applied to detect the content of Fe(II) in seawater.

## 1. Introduction

Iron is an important micronutrient for almost all organisms [1,2]. The overuse of iron may cause serious problems in some conditions, such as liver damage, kidney failure, etc. although iron is an essential element for all life [3]. In oxic systems, iron ions exist at extremely low concentrations because of the limited solubility of oxyhydroxide and particulate forms of iron [4]. In seawater, iron exists in two oxidation states: Fe(II) and Fe(III), and the former is more water-soluble, and is found in anoxic and suboxic waters such as deep lakes and isolated waters [5,6]. In river water, Fe(III) was mixed in estuarine water and delivered into the sea, and in this way, estuaries can act as one source of Fe(II) in seawater [7]. Fe(II) is easily oxidized into insoluble Fe(III) in oxic water [8], thus it is essential to recognize the role of Fe(II) in marine environments to better study the effects of redox iron species on marine microorganisms. Since the concentration of iron in seawater is relatively low, it is a challenge to accurately measure the iron content during environmental analysis.

Fe(II) can be detected by many methods such as spectrophotometry [9–11], fluorescence [12,13], phosphorescence [14], etc. Although these methods have serious of advantages, they are usually inconvenient, expensive, and time-consuming [15]. Comparatively, electro-analytical techniques, such as square wave stripping voltammetry (SWV) is an efficient technique for detecting trace Fe(II) and other heavy metals owing to its high sensitivity and selectivity, portability, low cost, and excellent performance with seawater [16,17]. Many studies on the determination of Fe(III) had been published [18–20]. However, only few electrochemical sensors for determination of Fe(II) had been explored. Berg, et al. reported an indirect method to analyze Fe(II) by masking it with bipyridyl as a complexant [6,8]. Mesquita et al. reported a polyaniline modified graphite electrode to detect Fe(II) with a limit of detection (LOD) of 1.90 mM [21]. Gholivand, et al. reported a carbon paste electrode (GCE) modified with dithiodianiline (DTDA) and gold nanoparticles (AuNPs) to detect Fe(II) with the LOD of 50 nM [22]. Disposable screen printed electrode modified with imine receptor having a wedge bridge for selective detection of Fe (II) in

\* Correspondence to: D. Pan, Key Laboratory of Coastal Environmental Processes and Ecological Remediation, Yantai Institute of Coastal Zone Research, Chinese Academy of Sciences, Yantai 264003, PR China.

\*\* Corresponding author.

E-mail addresses: [dwpn@yic.ac.cn](mailto:dwpn@yic.ac.cn) (D. Pan), [Kangqi@sdnu.edu.cn](mailto:Kangqi@sdnu.edu.cn) (Q. Kang).

<https://doi.org/10.1016/j.microc.2019.104210>

Received 3 March 2019; Received in revised form 31 July 2019; Accepted 24 August 2019

Available online 24 August 2019

0026-265X/ © 2019 Elsevier B.V. All rights reserved.

aqueous medium was used by Sonia, with the LOD of 0.54  $\mu\text{M}$  [23]. In our previous work, a dual nanomaterial-modified electrode for voltammetric stripping determination of trace Fe(II) in coastal waters with a LOD of 0.03 nM was reported [24], but the process of making electrodes was rather complicated. The electrochemical detection of Fe(II) is feasible, but how to lower the detection limit is still a popular topic. Increasing the surface area of the modified electrode seems to be a good way to solve this problem. There are two main strategies to increase the surface area of the modification material. One is to grow the material directly on the electrode by electrodeposition, but this method makes it difficult to control the morphology of the material. The other way to synthesize a material with a controllable morphology is using self-assembly [25].

Reduced graphene oxide (rGO) is usually obtained by the chemical/electrochemical reduction of graphene oxide (GO). Recently, rGO was used to improve the performance of electrochemical sensors, because it has high theoretical surface area [26]. Despite the great application potential, graphene possesses zero band gap and inertness to reaction, which reduced the competitive strength of graphene in the field of semiconductors and sensors. It meant that rGO needs decoration with other materials to improve its properties. Researchers had devoted efforts toward designing and constructing reduced graphene oxide-derived nanomaterials to make rGO with superior properties. Many functional nanocomposites derived from rGO had been reported in catalysts [27–29], sensors [30], electrochemical energy storage [31–33], etc. rGO modified with noble metal nanoparticles (NPs) had been used for electrochemical detection because noble metal NPs exhibited high catalytic activity via the size effect [34,35]. Platinum NPs were widely applied for detection of metal ions due to the high surface reaction activity, strong adsorption ability and ability to accelerate the catalytic process of PtNPs [36]. Methylene blue (MB) is a cationic thiazine dye and is widely used in many applications like aqua culture, chemotherapeutics, and medicine [37]. According to previous work [34,38], MB has many  $\pi$  electrons, and it will bind together by  $\pi$ - $\pi$  interactions with GO, which could avoid the aggregation of GO and increase the dispersity. MB adsorbed on the surface of the GO could attract  $\text{PtCl}_6^{2-}$ , allowing MB to act as the anchor for  $\text{PtCl}_6^{2-}$ , uniformly distributing  $\text{PtCl}_6^{2-}$  on the surface of MB, and increasing the GO dispersity. It is well-known that dyes are a major environmental concern, and metal nanoparticles (NPs) are often used as catalysts in catalytic dyes. Among the various metal NPs, PtNPs had good catalytic capacity for Fe(II) [20]. So, PtNPs was chosen in this work. The Langmuir–Hinshelwood approach can be used to describe the mechanism of catalytic reactions. This mechanism assumes that prior to a reaction, a dye will first be adsorbed on the surface of the NPs (catalyst), and the nanoparticles will act as an electron transfer media, and then the electrons transfer from the  $\text{BH}_4^-$  through the metal to reduce methylene blue and graphene oxide [39]. In other words, the electron transfer step is vital to many homogeneous and heterogeneous reactions. In this step, a large redox potential difference will exist between the donor and acceptor which may restrict the passage of electrons. An effective catalyst should possess an intermediate redox potential value between the donor and acceptor, which can accelerate the electron transfer and act as an electron relay system [40].

Herein, we fabricated the rGO/LMB/PtNPs/GCE modified electrode for determination of Fe(II). To prepare the nanocomposites, cationic dye of MB was adsorbed on the surface of GO with negatively charged, which is favorable to the self-assembly of  $\text{PtCl}_6^{2-}$  on the surface of GO/MB. After adding the reductant of  $\text{NaBH}_4$ , the composites of rGO/LMB/PtNPs was obtained. Where LMB is the abbreviation of leucomethylene blue. Thus, the rGO/LMB/PtNPs/GCE modified electrode was fabricated in situ. In the presence of 2,2'-bipyridyl (Bp), the sensitivity and selectivity of the as-prepared rGO/LMB/PtNPs/GCE to Fe(II) were improved significantly. This modified electrode was also applied to detect Fe(II) in real coastal water samples with satisfactory results.

## 2. Experimental

### 2.1. Reagents

All reagents used are of analytical grade or better. Chloroplatinic acid ( $\text{H}_2\text{PtCl}_6$ ) was purchased from Sinopharm Chemical Reagent Co., Ltd. (China). Graphene oxide was purchased from Nanjing XFNANO Materials Tech Co., Ltd. Methylene blue, iron sulfate heptahydrate, and 2,2'-bipyridyl were purchased from Sigma-Aldrich (Shanghai, China). Iron sulfate was dissolved in 0.01 M HCl to prepare an iron stock solution, and a new Fe(II) solution was prepared before each experiment. Standard artificial seawater (salinity of 4.998, 29.998, and 34.999) were purchased from Beijing Putian Tongchuang Biological Technology Co. Deionized water (with specific resistance of 18.2  $\text{M}\Omega\text{cm}$ ) was supplied by Pall Cascada laboratory water system. Unless stated otherwise, the electrochemical experiment was carried out in a 0.1 M acetate buffer (pH 4.5).

### 2.2. Apparatus

All electrochemical experiments were performed with an electrochemical work station (CHI 660E, CH Instruments, Inc., Shanghai, China) using a conventional three-electrode cell. A glassy carbon electrode (3 mm in diameter, Chenhua instruments, Shanghai, China) was used as the working electrode, with Ag/AgCl and platinum foil serving as the reference and counter electrodes, respectively. Polarographs (VA 797 Metrohm) were used for comparative testing. Scanning electron microscopy (SEM, Hitachi S-4800, Japan) and transmission electron microscopy (TEM, Oxford XMAX 80T) were used to observe the morphology of the nanomaterials, X-ray photoelectron spectroscopy (XPS) measurements were carried out on a photoelectron spectrometer (Escalab 250 Xi). X-ray diffraction (XRD) was performed using an X-ray diffractometer (D8, ADVANCE). UV–Vis spectra were measured in a spectrophotometer (DU 800, USA).

### 2.3. Preparation of rGO/LMB/PtNPs nanocomposites

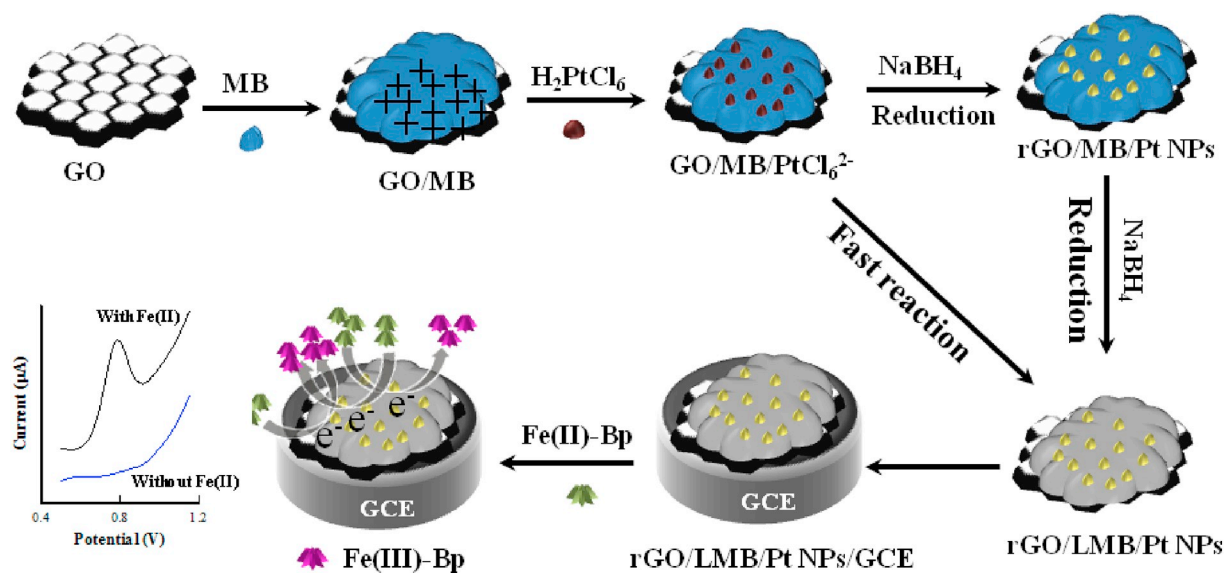
The synthesis process of rGO/LMB/PtNPs nanocomposites was showed in Scheme 1. Firstly, 20 mg GO was added into 30 mL deionized water and sonicated for 1 h until a uniform solution was obtained. Then 4 mL MB (1 mM) was added to the GO solution and stirred for 30 min, yielding the GO/MB nanocomposites. Afterwards, 1 mL of  $\text{H}_2\text{PtCl}_6$  solution (10 mM) was added and the mixture was magnetically stirred for 10 min. Finally, cautiously added, dropwise, 2 mL  $\text{NaBH}_4$  (0.20 M) solution and magnetically stirred for an additional 30 min to reduce GO, MB and  $\text{PtCl}_6^{2-}$ , yielding rGO/LMB/PtNPs. The as-prepared nanocomposites were collected by centrifugation, washed with deionized water, and dried in a vacuum drying chamber (70  $^\circ\text{C}$ ) for 1 h.

### 2.4. Preparation of rGO/LMB/PtNPs/GCE and electrochemical analysis

Prior to modification, the GCE was polished with 0.3  $\mu\text{m}$  and 0.05  $\mu\text{m}$  aqueous slurry of alumina powder, and sonicated for 3 min in ethanol and water, respectively. After dried in a stream of nitrogen, 10  $\mu\text{L}$  rGO/LMB/PtNPs (0.4  $\text{mg mL}^{-1}$ ) was spread on the surface of GCE and dried under an infrared light. The as-prepared rGO/LMB/PtNPs/GCE was used to detect Fe(II) by an SWV method. The following parameters were used in the SWV: deposition potential of  $-0.1$  V, deposition time of 90 s, scan potential 0.4  $\sim$  1.4 V, amplitude of 0.025 V, increment potential of 0.004 V, frequency of 15 Hz, and quiet time of 2 s.

### 2.5. Determination of Fe(II) in real seawater samples

Seawater samples were collected from the Dong Ying Station (Dongying City, Shandong Province, China), and stored in Teflon



**Scheme 1.** Schematic illustration of the fabrication process of rGO/LMB/PtNPs/GCE and determination of Fe(II).

bottles at 4 °C before determination. Prior to detection, N<sub>2</sub> was bubbled into the water samples and filtered through 0.45 µm membrane (Millipore). After adding 0.1 M acetate buffer (pH 4.5) and 60 µM Bp in the water sample, the concentration of the Fe(II) was detected by the aforementioned SWV method using rGO/LMB/PtNPs/GCE as the working electrode.

### 3. Results and discussion

#### 3.1. Characterization of rGO/LMB/PtNPs

The TEM and SEM images of rGO, rGO/MB and rGO/LMB/PtNPs were shown in Fig. 1. It can be seen that the as-prepared rGO and rGO/MB exhibit a pleated surface and black misty structure, respectively. Because MB can provide a positively-charged site for the uniform dispersion of PtCl<sub>6</sub><sup>2-</sup>, PtNPs were uniformly dispersed on the surface of the rGO/MB-based substrate after a reduction reaction with NaBH<sub>4</sub> (Fig. 1C & D). In addition, part of PtNPs were sandwiched within the rGO/LMB, which could enhance the conductivity and catalytic performance of the nanocomposites. As can be seen from the XPS spectra in Fig. S1 in Electronic Supplementary Material (ESM), N 1s, S 2p and Pt 4f peaks were occurred in the rGO/LMB/PtNPs composite. The EDS pattern of rGO/LMB/PtNPs in Fig. 1E also indicated that C, O, Pt, and S were the major elements in the composites. The C, O and S might come from rGO and LMB, Na from aluminum foil. The peak of Pt reveals the existence of PtNPs. Thus, LMB and PtNPs were proven to conjugate on the surface of rGO.

XRD is an effective method to investigate interlayer changes and crystalline properties of nanomaterials. As shown in Fig. 1F, GO exhibited a prominent diffraction peak at about  $2\theta = 10.9$  deg. (001), which was identical to a reported value [41]. The as-prepared rGO had a slight shorter peak at (001) ( $2\theta = 9.7$  deg.), implying that the reduction of GO by NaBH<sub>4</sub> could remove the oxygen-containing functional groups. In addition, there was a small peak at (002) ( $2\theta = 22.7$  deg.). According to the Prague formula, oxygen-containing functional groups were presented on the surface of the GO, and the inter-layer d-spacing of GO was calculated to be 0.81 nm. As oxygen-containing functional groups were presented on the surface of GO, it could easily form a large interlayer d-spacing, causing the formation of the diffraction peak (002). In the composite of rGO/LMB/PtNPs, the (001) peak was nearly disappeared, implying the catalytic activity of PtNPs in the reduction of GO. The lattice planes of the platinum face-centered cubic crystal (111) appeared at typical diffraction peaks at

$2\theta = 38.13$  deg. Compared with rGO/MB, the interlayer d-spacing of the rGO/LMB/PtNPs was increased to 0.36 nm ( $2\theta = 24.7$  deg.) due to PtNPs entering into the interlayer spaces of rGO [42]. The insertion of PtNPs into the composites played an important role in the anodic response to Fe(II)-Bp.

Fig. S2 showed the UV-Vis spectrum of the rGO/LMB/PtNPs composites. It can be seen that the absorption peaks of MB at 660 and 289 nm were obviously changed as MB was reduced to LMB in the composites. The absorption peak at 675 nm indicated that LMB was adsorbed on the rGO surface [34]. In addition, the typical absorption peak of GO at 223 nm [43] was disappeared and the absorption peak of rGO at 261 nm was occurred, suggesting the existence of rGO in the composites.

#### 3.2. Electrochemical behaviors of rGO/LMB/PtNPs/GCE

The comparison between the different modified electrodes was investigated in an acetate buffer (0.1 M, pH 4.5). To increase the selectivity and sensitivity for Fe(II) determination, Bp was used as the complexing agent to form the complex of [Fe(Bp)<sub>3</sub>]<sup>2+</sup>. Firstly, cyclic voltammetry (CV) was used to verify the effect of the modified electrode on Fe(II) detection. The CV response curves of different electrodes are shown in Fig. S3. It can be seen that only very weak redox peaks can be observed on bare GCE. In the case of rGO/GCE, the redox peaks were enhanced due to the electrocatalytic activity of rGO. When the rGO/MB/GCE electrode was used, the redox peaks were enhanced further because MB, as an electron mediator, would accelerate the electron transfer. As expected, the redox peaks were much enhanced in rGO/LMB/PtNPs/GCE, indicating that LMB and PtNPs could synergistically improve the anodic current response of Fe(II)-Bp. Hence, rGO/LMB/PtNPs/GCE electrode could be used to detect Fe(II) with the help of 2,2'-bipyridyl.

The dependence of the peak current in cyclic voltammograms of rGO/LMB/PtNPs/GCE on scan rate were shown in Fig. S4. It can be seen that cathodic ( $I_{pc}$ ) and anodic ( $I_{pa}$ ) peak currents were in linear correlations with scan rate, indicating that the electro-anode reactions of Fe(II)-Bp at the rGO/LMB/PtNPs/GCE surface were typical adsorption controlled processes [44].

Because higher sensitivity can be obtained by square wave voltammetry (SWV) than that by CV, the SWV responses of the rGO/LMB/PtNPs/GCE was also investigated. As shown in Fig. 2, the bare GCE and PtNPs/GCE had little response to low concentration of Fe(II)-Bp (curves a and c). In rGO/GCE, a small anodic peak near 0.8 V was observed due

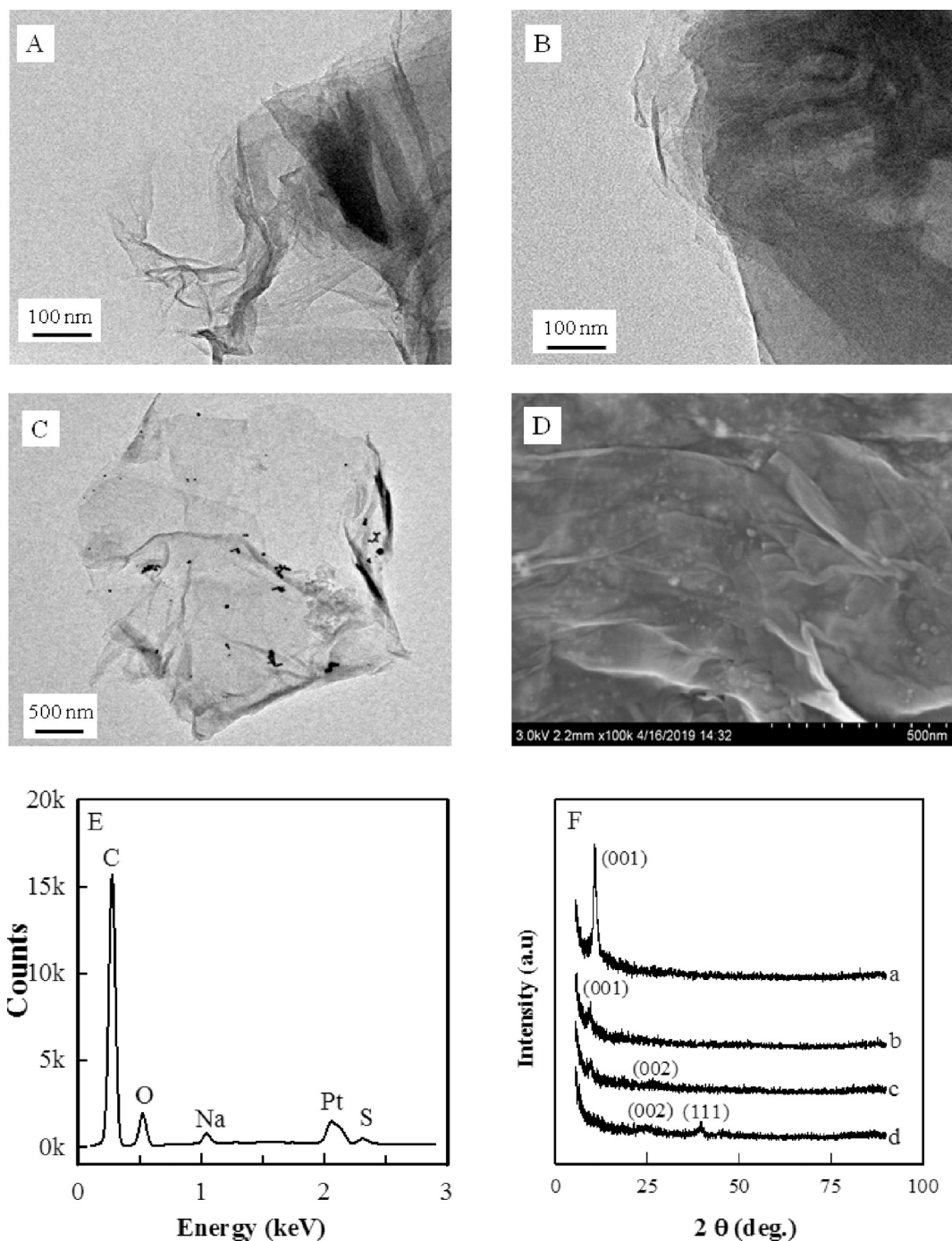


**Fig. 1.** TEM images of rGO (A), rGO/MB (B) and rGO/LMB/PtNPs (C), SEM images (D) and EDS pattern (E) of rGO/LMB/PtNPs, and XRD patterns (F) of GO (a), rGO (b), rGO/MB (c), and rGO/LMB/PtNPs (d) composites.

to the electrocatalytic activity of rGO (curve b). In the cases of rGO/PtNPs/GCE and rGO/MB/GCE, the current responses were enhanced but the shapes of the voltammograms were irregular (curves d and e). In the square wave stripping analysis, PtNPs had high catalytic activity to Fe (II) while rGO were employed as a support material and also could transfer electrons acquired from the catalytic process of the PtNPs to electrodes, which might accelerate the catalytic process. Therefore, rGO/PtNPs modified GCE had a higher peak current compared to only PtNPs modified GCE at about 0.8 V. Meanwhile, MB, as an electron mediator, would accelerate the electron transfer, which could promote the transformation from  $[\text{Fe}(\text{Bp})_3]^{2+}$  to  $[\text{Fe}(\text{Bp})_3]^{3+}$  [39]. rGO/LMB/PtNPs/GCE (curve f) also had an obvious higher SWV current response

than rGO/MB/GCE, indicating that synergistic and catalytic effects could notably improve the response of this fabricated electrode to Fe (II). The structure of LMB was the same as phenothiazine [45] and it was a bridge to connect the rGO and PtNPs. It was easy to find that the peak potential of target modified electrode shifted to the right compared with other peaks. In other words,  $[\text{Fe}(\text{Bp})_3]^{2+}$  was more easily oxidized on the target modified electrode.

As shown in Scheme 1, Fe(II)-Bp was electrodeposited onto the surface of rGO/LMB/PtNPs/GCE. Hence, Bp has obvious effect on the response of rGO/LMB/PtNPs/GCE. Although Bp itself has no obvious redox signal in the potential range used (Fig. 3b). In the absence of Bp, the response of rGO/LMB/PtNPs/GCE to Fe(II) was very weak (Fig. 3c).

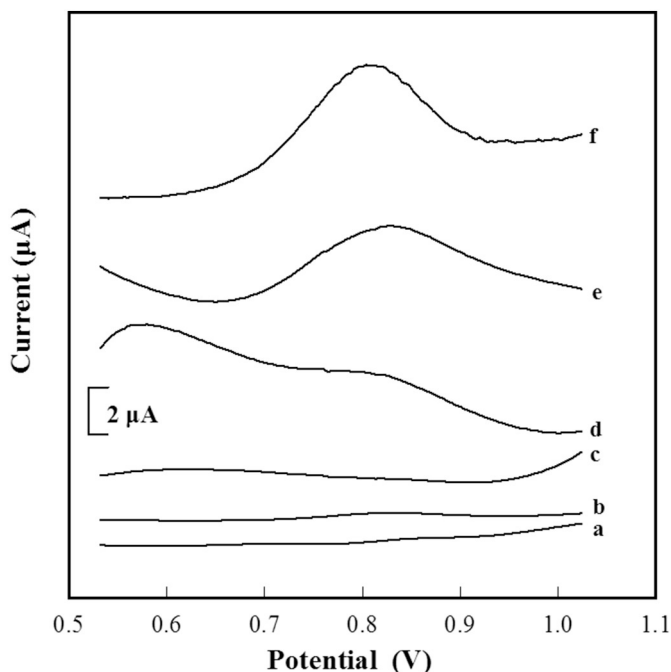


Fig. 2. SWV response curves of bare GCE (a), rGO/GCE (b), PtNPs/GCE (c), rGO/PtNPs/GCE (d), rGO/MB/GC (e) and rGO/LMB/PtNPs/GCE (f) in 0.1 M acetate buffer (pH 4.5) containing 60  $\mu\text{M}$  Bp and 2  $\mu\text{M}$  Fe(II).

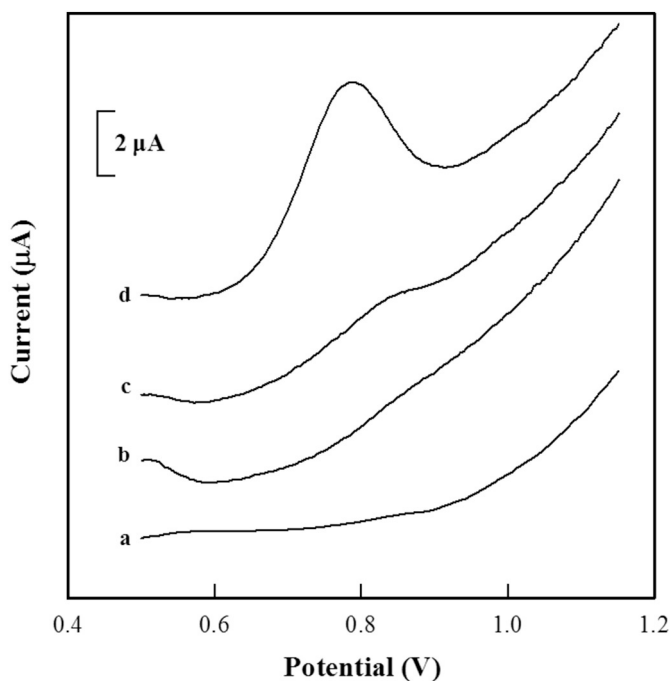


Fig. 3. SWV response curves of rGO/LMB/PtNPs/GCE in different solutions. (a) 0.1 M acetate buffer (pH 4.5), (b) 0.1 M acetate buffer (pH 4.5) and 60  $\mu\text{M}$  Bp, (c) 0.1 M acetate buffer (pH 4.5) and 2  $\mu\text{M}$  Fe(II), (d) 0.1 M acetate buffer (pH 4.5) containing 60  $\mu\text{M}$  Bp and 2  $\mu\text{M}$  Fe(II).

After the addition of Bp, the peak current was 7.5 times than that without Bp (Fig. 3d). During the process of electrochemical deposition, Fe(II)-Bp might be adsorbed onto the surface of rGO/LMB/PtNPs/GCE. The complex followed a simple one-electron transfer process in aqueous solution. The specific mechanism was reported by Lin et al. using Fourier transformed alternating current (FTAC) voltammetry [46].

### 3.3. Optimization for Fe(II) determination using rGO/LMB/PtNPs/GCE

To obtain a better analytical performance for Fe(II) determination, the main experimental conditions were optimized. As shown in Fig. S5A, the peak current was increased with increasing pH value in the range from 3.5 to 4.5 then decreased at higher pH value. The reason is that Fe(II) can be easily oxidized under weakly acidic or alkaline conditions. On the other hand, Fe(II)-Bp could not exist stably under neutral or alkaline conditions. Hence, the pH value of 4.5 was used for Fe(II) determination. In the concentration range from 0.05 to 0.4 M, the peak current of rGO/LMB/PtNPs/GCE was related slightly to the concentration of acetate buffer (Fig. S5B in ESM). Accordingly, the acetate buffer (0.1 M, pH 4.5) were used in this work.

The dependence of the response of rGO/LMB/PtNPs/GCE to Fe(II) on the content of modifier was depicted in Fig. S6A. It can be seen that the maximum response signal was obtained at the concentration of 0.4  $\text{mg mL}^{-1}$ . Hence, 10  $\mu\text{L}$  of 0.4  $\text{mg mL}^{-1}$  rGO/LMB/PtNPs were used to fabricate the modified electrode in this work. As shown in Fig. S6B, with the concentration of Bp increased from 30 to 60  $\mu\text{M}$ , the response signal was increased slightly then decreased at higher concentration. Too much free Bp would compete with Fe(II)-Bp to adsorb on the modified electrode. Therefore, 60  $\mu\text{M}$  of Bp was chosen for Fe(II) determination.

To obtain better stripping response, the deposition potential of Fe(II)-Bp at the modified electrode was investigated in the range from  $-0.4$  V to 0 V. As shown in Fig. S7A in ESM, with deposition potential of  $-0.1$  V, the modified electrode showed a better current response. Additionally, an increase in the peak current was observed when the potential gradually increased from  $-0.4$  to  $-0.1$  V, which was likely due to the strong adsorption of the positively-charged Fe(II)-Bp complex onto the surface of the modified electrode, since rGO/LMB/PtNPs had a negative charge. However, the peak current showed a decrease as the potential increased from  $-0.1$  to 0 V, which was due to a sufficient amount of positively-charged Fe(II)-Bp complex not being adsorbed on the surface of the negatively-charged modified electrode. Thus, such deposition potential was used for Fe(II) determination. As shown in Fig. S7B in ESM, the response signal was increased near-linearly with increasing deposition time from 15 s to 60 s, and then tended to increase slowly. Therefore, 90 s was chosen in the following SWV method for Fe(II) determination.

### 3.4. Analytical performance in Fe(II) detection

Under optimized experimental conditions, the calibration curve of Fe(II) determination using rGO/LMB/PtNPs/GCE by SWV method was shown in Fig. 4. The concentration of Fe(II) was studied in the range of 0.01  $\sim$  8  $\mu\text{M}$ . The results showed that it had a good linear relationship in the range of 0.01 to 2  $\mu\text{M}$ . The linear regression equation was  $I_p = 1.7105C + 0.5531$  ( $R^2 = 0.996$ ), where  $I_p$  is the peak current and  $C$  is the concentration of Fe(II) ( $\mu\text{M}$ ). The sensitivity was 1.71  $\mu\text{A}/\mu\text{M}$ , with the LOD of 3 nM ( $S/N=3$ ). Additionally, the comparison of the analytical performance between the proposed method and some other analytical methods was listed in Table 1, indicating that the proposed method offers an acceptable sensitivity and linear range for Fe(II) determination. The selectivity of the proposed electrode was tested and demonstrated in Fig. 5. Under the experimental conditions used, for the determination of 2  $\mu\text{M}$  Fe(II), 50-fold Cr(III), Zn(II), Ag(I), 40-fold Co(III), Pb(II), Mg(II), 20-fold Cd(II), Hg(II), and 10-fold amounts of Cu(II) and Bi(III) had negligible interfere ( $< 5\%$  of response current change). The good selectivity was based on the fact that Fe(II) can form a strong bond with Bp in weak acidic solution conditions. The complex of Fe(II)-Bp can be enriched on the surface of rGO/LMB/PtNPs/GCE in an SWV process.

In addition, the reproducibility of the rGO/LMB/PtNPs/GCE was tested in the solution containing 2  $\mu\text{M}$  Fe(II) and 60  $\mu\text{M}$  Bp. It was shown that the relative standard deviation (RSD) of the response signals

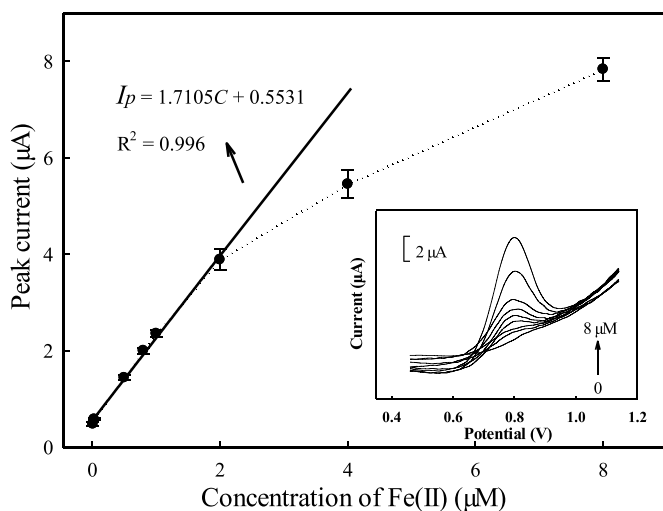


Fig. 4. The calibration curve for Fe(II) detection. Inset: SWV voltammograms of the rGO/LMB/PtNPs/GC in 0.1 M acetate buffer (pH 4.5) containing different Fe(II) concentrations (from 0.01 to 2  $\mu\text{M}$ ). Scan rate: 25  $\text{mV}\cdot\text{s}^{-1}$ .

among five independently-modified electrodes was 4.0%, implying that the as-fabricated rGO/LMB/PtNPs/GCE offers an acceptable reproducibility. On the other hand, the RSD of eight parallel determinations by using the same electrode was 4.9%, revealing an acceptable repeatability in continuous determination.

### 3.5. Detection of Fe(II) in seawater samples

To evaluate the practical application of the established electrode, the rGO/LMB/PtNPs/GCE was employed to detect Fe(II) in standard artificial and seawater samples. As listed in Table 2, the amounts of Fe(II) in three real seawater samples 1 was calculated to be 23.3 nM, and in seawater sample 2 and sample 3, the concentrations were calculated to be 20.6 nM and 51.1 nM, respectively. Because the concentration of Fe(II) in seawater was very low and the determination of Fe(II) needed special treatment, the results were agreed with those measure by a reference method based on catalytic cathodic stripping voltammetry (CSV) [24]. In addition, the recoveries in a standard addition method were in the range of 92 ~ 101% in the real and artificial seawater samples. These results illustrated that the fabricated electrode had a good applicability for Fe(II) determination in real water samples.

Table 1

Comparison of the analytical performance of the proposed electrochemical sensor with other methods for Fe(II) determination.

Methods <sup>a</sup>	Electrode/agents <sup>b</sup>	Linear range (nM)	Detecting limit (nM)	Sensitivity ( $\mu\text{A}/\mu\text{M}$ )	References
Colorimetry	FTO coated glass	–	5357.10	NC <sup>c</sup>	[14]
Colorimetry	Silica sol	1250–25,535.70	285.70	NC	[9]
Phosphorimetry	MPA-Mn: ZnS-QDs	10–10,000	3	–	[12]
Fluorometry	Au <sub>7</sub> (DHLA) <sub>2</sub> Cl <sub>2</sub>	–	3800	–	[10]
CSV	HMDE	–	0.12	–	[6]
CV	PANI/G	892.86–892,860	267.90	0.03	[21]
DPV	SPE	600–4000	540	1.27	[23]
DPASV	DTDA/AuNPs/CPE	10–100	0.05	4	[22]
SWV	TiCNPs-Nafion/PtNFs/GCE	10–6000	0.03	5.02	[24]
SWV	rGO/LMB/PtNPs/GCE	10–2000	3	1.71	Present work

<sup>a</sup> Methods: CSV, catalytic cathodic stripping voltammetry; DPV, differential pulse voltammograms; DPASV, differential pulse anodic stripping voltammetry.

<sup>b</sup> Electrode/reagents: FTO, fluorine-doped tin oxide; MPA-Mn: ZnS-QDs, phosphorescent 3-mercaptopropionic acid (MPA) capped Mn-doped ZnS quantum dots; HMDE, hanging mercury drop electrode; PANI/G, polyaniline/graphite; SPE, screen printed electrodes; DTDA/AuNPs/CPE, dithiodianiline/gold nanoparticles/carbon paste electrode; TiCNPs-Nafion/Pt NFs, titanium carbide nanoparticles-Nafion/platinum nanoflowers.

<sup>c</sup> NC: not comparable.

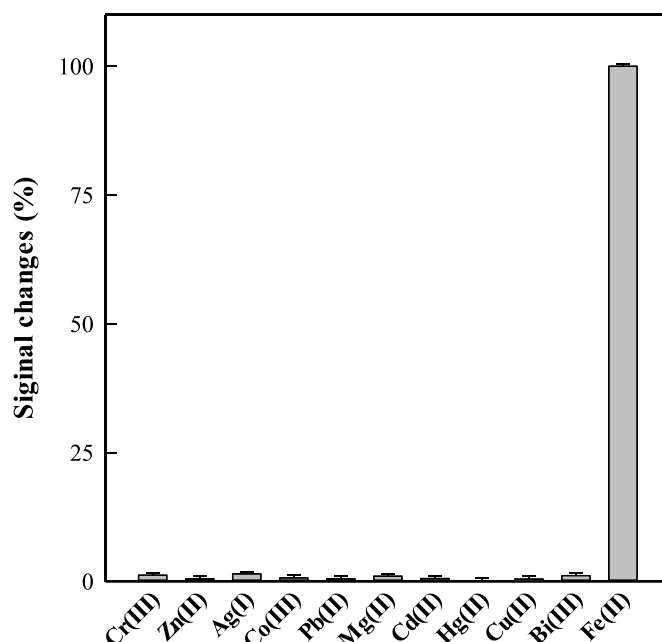


Fig. 5. The interference of other metal ions to Fe(II) detection. Experimental conditions: 0.1 M acetate buffer (pH 4.5) containing 60  $\mu\text{M}$  Bp and 2  $\mu\text{M}$  Fe(II). Concentration of other metal ions: 50-fold Cr(III), Zn(II), Ag(I), 40-fold of Co(III), Pb(II) and Mg(II), 20-fold Cd(II) and Hg(II), and 10-fold of Cu(II) and Bi(III).

## 4. Conclusions

In summary, a novel and effective rGO/LMB/PtNPs-modified GCE was used for the sensitive determination of Fe(II), which obtained a good detection effect upon real sample. Compared to other electrochemical sensors, the modified electrode in this work had a lower detection limit, good reproducibility, repeatability, and selectivity. It was facile to fabricate the rGO/LMB/PtNPs. GO and MB combined with each other by mutual  $\pi$ - $\pi$  interactions. The cationic dye MB had a slight positive charge and could be combined with  $\text{PtCl}_6^{2-}$  through opposite charge interactions. By using  $\text{NaBH}_4$  as the reducing agent in the presence of PtNPs, the MB (blue) could be degraded into LMB (colorless), and the GO was reduced to rGO. In summary, the electrode fabricated in this work was reliable and suitable for determination of Fe(II) in actual seawater.

**Table 2**  
Determination of Fe(II) in standard artificial and real seawater samples by the proposed and catalytic CSV methods.

Samples	Fe(II) added (nM)	Proposed method		Catalytic CSV (nM)
		Mean <sup>a</sup> ± SD (nM)	Recovery (%)	
Sample 1	0	23.3 ± 2.4		20.0 ± 4.1
	10.0	32.8 ± 2.6	95	
Sample 2	0	20.6 ± 1.6		21.1 ± 3.9
	10.0	29.8 ± 2.0	92	
Sample 3	0	51.1 ± 3.5		46.2 ± 5.7
	10.0	60.3 ± 3.2	92	
Artificial seawater 1 <sup>b</sup>	0	ND <sup>c</sup>		
	50.0	50.4 ± 1.7	101	
	100	100.2 ± 1.5	100	
Artificial seawater 2	0	ND		
	50.0	49.6 ± 2.5	99	
	100	96.4 ± 2.3	96	
Artificial seawater 3	0	ND		
	50.0	46.3 ± 3.3	93	
	100	95.0 ± 3.2	95	

<sup>a</sup> Mean is calculated from three determinations.

<sup>b</sup> The salinities of the standard artificial seawater samples 1, 2 and 3 are 4.998, 20.998 and 34.999, respectively.

<sup>c</sup> Not detected.

## Acknowledgements

This work was financially supported by the National Natural Science Foundation of China (21874083), the National Natural Science Foundation (ZR2018MB029) and Key Research and Development Plan of Shandong Province (2017GHY215002), the Key Research and Development Plan of Yantai City (2017ZH096).

## Appendix A. Supplementary data

Supplementary data to this article can be found online at <https://doi.org/10.1016/j.microc.2019.104210>.

## References

- A. Kustka, E.J. Carpenter, S.A. Sañudo-Wilhelmy, Iron and marine nitrogen fixation: progress and future directions, *Res. Microbiol.* 153 (2002) 255–262, [https://doi.org/10.1016/S0923-2508\(02\)01325-6](https://doi.org/10.1016/S0923-2508(02)01325-6).
- S. Rana, S.K. Mittal, N. Kaur, C.E. Banks, Disposable screen printed electrode modified with imine receptor having a wedge bridge for selective detection of Fe(II) in aqueous medium, *Sensors Actuators B Chem.* 249 (2017) 467–477, <https://doi.org/10.1016/j.snb.2017.04.135>.
- A. Kamal, N. Kumar, V. Bhalla, M. Kumar, R.K. Mahajan, Rhodamine-dimethyliminocinnamyl based electrochemical sensors for selective detection of iron (II), *Sensors Actuators B Chem.* 190 (2014) 127–133, <https://doi.org/10.1016/j.snb.2013.08.079>.
- J.H. Martin, M. Gordon, S.E. Fitzwater, The case for iron, *Limnol. Oceanogr.* 36 (1991) 1793–1802, <https://doi.org/10.4319/lo.1991.36.8.1793>.
- E. Breitbarth, J. Gelting, J. Walve, L.J. Hoffmann, D.R. Turner, M. Hasselöv, J. Ingri, Dissolved iron(II) in the Baltic Sea surface water and implications for cyanobacterial bloom development, *Biogeosciences* 6 (2009) 2397–2420, <https://doi.org/10.5194/bg-6-2397-2009>.
- M. Gledhill, C.M.G.V.D. Berg, Measurement of the redox speciation of iron in seawater by catalytic cathodic stripping voltammetry, *Mar. Chem.* 50 (1995) 51–61, [https://doi.org/10.1016/0304-4203\(95\)00026-N](https://doi.org/10.1016/0304-4203(95)00026-N).
- M.J. Hopwood, P.J. Statham, A. Milani, Dissolved Fe(II) in a river-estuary system rich in dissolved organic matter, *Estuar. Coast. Shelf Sci.* 151 (2014) 1–9, <https://doi.org/10.1016/j.ecss.2014.09.015>.
- A.P. Aldrich, C.M.G.V.D. Berg, Determination of iron and its redox speciation in seawater using catalytic cathodic stripping voltammetry, *Electroanalysis* 10 (2015) 369–373, [https://doi.org/10.1002/\(SICI\)1521-4109\(199805\)10:6<369::AID-ELAN369>3.0.CO;2-W](https://doi.org/10.1002/(SICI)1521-4109(199805)10:6<369::AID-ELAN369>3.0.CO;2-W).
- S. Metarwiwinit, S. Mukdasai, C. Poonsawat, S. Srijaranai, A simple dispersive-micro-solid phase extraction based on a colloidal silica sorbent for the spectrophotometric determination of Fe(II) in the presence of tetrabutylammonium bromide, *New J. Chem.* 42 (2018) 3401–3408, <https://doi.org/10.1039/C7NJ04172A>.
- D.A. Ondigo, Z.R. Tshentu, N. Torto, Electrospun nanofiber based colorimetric probe for rapid detection of Fe<sup>2+</sup> in water, *Anal. Chim. Acta* 804 (2013) 228–234, <https://doi.org/10.1016/j.aca.2013.09.051>.
- N.O. Laschuk, I.I. Ebralidze, S. Quaranta, S.T.W. Kerr, J.G. Egan, S. Gillis, F. Gaspari, A. Latini, O.V. Zenkia, Rational design of a material for rapid colorimetric Fe<sup>2+</sup> detection, *Mater. Des.* 107 (2016) 18–25, <https://doi.org/10.1016/j.matdes.2016.06.016>.
- L. Yang, J. Chen, T. Huang, L. Huang, Z. Sun, Y. Jiang, T. Yao, S. Wei, Red-emitting Au<sub>7</sub> nanoclusters with fluorescence sensitivity to Fe<sup>2+</sup> ions, *J. Mater. Chem. C* 5 (2017) 4448–4454, <https://doi.org/10.1039/C7TC00724H>.
- Y.W. Choi, G.J. Park, Y.J. Na, H.Y. Jo, S.A. Lee, G.R. You, C. Kim, A single schiff base molecule for recognizing multiple metal ions: a fluorescence sensor for Zn(II) and Al(III) and colorimetric sensor for Fe(II) and Fe(III), *Sensors Actuators B Chem.* 194 (2014) 343–352, <https://doi.org/10.1016/j.snb.2013.12.114>.
- Q. Jin, Y. Hu, Y. Sun, Y. Li, J. Huo, X. Zhao, Room-temperature phosphorescence by Mn-doped ZnS quantum dots hybrid with Fenton system for the selective detection of Fe<sup>2+</sup>, *RSC Adv.* 5 (2015) 41555–41562, <https://doi.org/10.1039/c5ra04026d>.
- M. Liu, D. Pan, W. Pan, Y. Zhu, X. Hu, H. Han, C. Wang, D. Shen, In-situ synthesis of reduced graphene oxide/gold nanoparticles modified electrode for speciation analysis of copper in seawater, *Talanta* 174 (2017) 500–506, <https://doi.org/10.1016/j.talanta.2017.06.054>.
- A. Afkhami, M. Soltani-Shahrivar, H. Ghaedi, T. Madrakian, Construction of modified carbon paste electrode for highly sensitive simultaneous electrochemical determination of trace amounts of copper (II) and cadmium (II), *Electroanalysis* 28 (2016) 296–303, <https://doi.org/10.1002/elan.201500308>.
- J.J. Silva, L.L. Paim, N.R. Stradiotto, Simultaneous determination of iron and copper in ethanol fuel using nafion/carbon nanotubes electrode, *Electroanalysis* 26 (2014) 1794–1800, <https://doi.org/10.1002/elan.201400136>.
- H. Han, D. Pan, C. Wang, R. Zhu, Controlled synthesis of dendritic gold nanostructures by graphene oxide and their morphology-dependent performance for iron detection in coastal waters, *RSC Adv.* 7 (2017) 15833–15841, <https://doi.org/10.1039/C6RA27075A>.
- F. Li, D. Pan, M. Lin, H. Han, X. Hu, Q. Kang, Electrochemical determination of iron in coastal waters based on ionic liquid-reduced graphene oxide supported gold nanodendrites, *Electrochim. Acta* 176 (2015) 548–554, <https://doi.org/10.1016/j.electacta.2015.07.011>.
- M. Lin, H. Han, D. Pan, H. Zhang, Z. Su, Voltammetric determination of total dissolved iron in coastal waters using a glassy carbon electrode modified with reduced graphene oxide, methylene blue and gold nanoparticles, *Electrochim. Acta* 182 (2015) 805–813, <https://doi.org/10.1007/s00604-014-1391-6>.
- C.S. Camacho, J.C. Mesquita, J. Rodrigues, Electrodeposition of polyaniline on self-assembled monolayers on graphite for the voltammetric detection of iron(II), *Mater. Chem. Phys.* 184 (2016) 261–268, <https://doi.org/10.1016/j.matchemphys.2016.09.050>.
- M.B. Gholivand, B. Geravandi, M.H. Parvin, Anodic stripping voltammetric determination of iron(II) at a carbon paste electrode modified with dithiodianiline (DTDA) and gold nanoparticles (GNP), *Electroanal.* 23 (2011) 1345–1351, <https://doi.org/10.1002/elan.201000715>.
- S. Rana, S.K. Mittal, N. Kaur, C.E. Banks, Disposable screen printed electrode modified with imine receptor having a wedge bridge for selective detection of Fe(II) in aqueous medium, *Sensors Actuators B Chem.* 249 (2017) 467–477, <https://doi.org/10.1016/j.snb.2017.04.135>.
- M. Lin, D. Pan, Y. Zhu, X. Hu, H. Han, C. Wang, Dual-nanomaterial based electrode for voltammetric stripping of trace Fe(II) in coastal waters, *Talanta* 154 (2016) 127–133, <https://doi.org/10.1016/j.talanta.2016.03.060>.
- W. Xiao, Y. Zhang, B. Liu, Raspberrylike SiO<sub>2</sub>@reduced graphene oxide@AgNP composite microspheres with high aqueous dispersity and excellent catalytic activity, *ACS Appl. Mater. Inter.* 7 (2015) 6041–6046, <https://doi.org/10.1021/acsami.5b00296>.
- X. Xuan, J.Y. Park, A miniaturized and flexible cadmium and lead ion detection sensor based on micropatterned reduced graphene oxide/carbon nanotube/bismuth composite electrodes, *Sensors Actuators B Chem.* 255 (2018) 1220–1227, <https://doi.org/10.1016/j.snb.2017.08.046>.
- H. Zhang, X. Lv, Y. Li, Y. Wang, J. Li, P25-graphene composite as a high performance photocatalyst, *ACS Nano* 4 (2010) 380–386, <https://doi.org/10.1021/nn901221k>.
- C. Zhu, S. Dong, Recent progress in graphene-based nanomaterials as advanced electrocatalysts towards oxygen reduction reaction, *Nanoscale* 5 (2013) 1753–1767, <https://doi.org/10.1039/c2nr33839d>.
- C. Zhu, P. Wang, L. Wang, L. Han, S. Dong, Facile synthesis of two-dimensional graphene/SnO<sub>2</sub>/Pt ternary hybrid nanomaterials and their catalytic properties, *Nanoscale* 3 (2011) 4376–4382, <https://doi.org/10.1039/c1nr10634a>.
- M. Zhou, Y. Zhai, S. Dong, Electrochemical sensing and biosensing platform based on chemically reduced graphene oxide, *Anal. Chem.* 81 (2009) 5603–5613, <https://doi.org/10.1021/ac900136z>.
- S.M. Paek, E.J. Yoo, I. Honma, Enhanced cyclic performance and lithium storage capacity of SnO<sub>2</sub>/graphene nanoporous electrodes with three-dimensionally delaminated flexible structure, *Nano Lett.* 9 (2009) 72–75, <https://doi.org/10.1021/nl802484w>.
- X. Zhu, Y. Zhu, S. Murali, M.D. Stoller, R.S. Ruoff, Nanostructured reduced graphene oxide/Fe<sub>2</sub>O<sub>3</sub> composite as a high-performance anode material for lithium ion batteries, *ACS Nano* 5 (2011) 3333, <https://doi.org/10.1021/nn200493r>.
- Y. Zhu, S. Murali, M.D. Stoller, K.J. Ganes, W. Cai, P.J. Ferreira, A. Pirkle, R.M. Wallace, K.A. Cychoz, T. Matthias, Carbon-based supercapacitors produced by activation of graphene, *Science* 332 (2011) 1537, <https://doi.org/10.1126/science.1200770>.
- H. Han, D. Pan, X. Wu, Q. Zhang, H. Zhang, Synthesis of graphene/methylene blue/

- gold nanoparticles composites based on simultaneous green reduction, in situ growth and self-catalysis, *J. Mater. Sci.* 49 (2014) 4796–4806, <https://doi.org/10.1007/s10853-014-8179-2>.
- [35] B. He, H. Liu, Electrochemical determination of nitrofurans residues at gold nanoparticles/graphene modified thin film gold electrode, *Microchem. J.* 150 (2019) 104108, <https://doi.org/10.1016/j.microc.2019.104108>.
- [36] Y. Zuo, J. Xu, X. Zhu, X. Duan, L. Lu, Y. Yu, Graphene-derived nanomaterials as recognition elements for electrochemical determination of heavy metal ions: a review, *Microchim. Acta* 186 (3) (2019), <https://doi.org/10.1007/s00604-019-3248-5>.
- [37] J. Saha, A. Begum, A. Mukherjee, S. Kumar, A novel green synthesis of silver nanoparticles and their catalytic action in reduction of methylene blue dye, *Sustain. Environ. Res.* 27 (2017) 245–250, <https://doi.org/10.1016/j.serj.2017.04.003>.
- [38] Y. Zhang, L. Liu, F. Xi, T. Wu, X. Lin, A simple layer-by-layer assembly strategy for a reagentless biosensor based on a nanocomposite of methylene blue-multiwalled carbon nanotubes, *Electroanal.* 22 (2010) 277–285, <https://doi.org/10.1002/elan.200900307>.
- [39] P. Ncube, N. Bingwa, H. Baloyi, R. Meijboom, Catalytic activity of palladium and gold dendrimer-encapsulated nanoparticles for methylene blue reduction: a kinetic analysis, *Appl. Catal. A* 495 (2015) 63–71, <https://doi.org/10.1016/j.apcata.2015.01.033>.
- [40] K. Mallick, M. Witcomb, M. Scurrill, Silver nanoparticle catalysed redox reaction: an electron relay effect, *Mater. Chem. Phys.* 97 (2006) 283–287, <https://doi.org/10.1016/j.matchemphys.2005.08.011>.
- [41] S. Gurunathan, J.W. Han, V. Eppakayala, J.H. Kim, Biocompatibility of microbially reduced graphene oxide in primary mouse embryonic fibroblast cells, *Colloid. Surface. B* 105 (2013) 58–66, <https://doi.org/10.1016/j.colsurfb.2012.12.036>.
- [42] Z. Wang, K. Shang, J. Dong, Z. Cheng, S. Ai, Electrochemical immunoassay for subgroup J of avian leukosis viruses using a glassy carbon electrode modified with a film of poly (3-thiophene boronic acid), gold nanoparticles, graphene and immobilized antibody, *Microchim. Acta* 179 (2012) 227–234, <https://doi.org/10.1007/s00604-012-0874-6>.
- [43] C. Shan, H. Yang, D. Han, Q. Zhang, A. Lvaska, L. Niu, Graphene/AuNPs/chitosan nanocomposites film for glucose biosensing, *Biosens. Bioelectron.* 25 (2010) 1070–1074, <https://doi.org/10.1016/j.bios.2009.09.024>.
- [44] Y. Hong, W. P. S. Huang, X. Gao, S. Song, W. Wang, X. Guo, Simultaneous electrochemical determination of levodopa and uric acid based on ZnS nanoparticles/3D graphene foam electrode, *Microchem. J.* 149 (2019) 103977.
- [45] S.H.D.A. Nicolai, P.R.P. Rodrigues, S.M.L. Agostinho, J.C. Rubim, Electrochemical and spectroelectrochemical (SERS) studies of the reduction of methylene blue on a silver electrode, *J. Electroanal. Chem.* 527 (2002) 103–111, [https://doi.org/10.1016/S0022-0728\(02\)00832-X](https://doi.org/10.1016/S0022-0728(02)00832-X).
- [46] M. Lin, J. Li, D. Pan, A.M. Bond, J. Zhang, A systematic study of the mass transport, kinetic and thermodynamic properties of the Fe (III/II) process at glassy carbon and boron-doped diamond electrodes, *Electrochim. Acta* 249 (2017) 421–430, <https://doi.org/10.1016/j.electacta.2017.07.155>.